

1

Introduction

As described in the Preface, the subject of this book is how to efficiently measure a gear and compute from these measurements the kinematic (force and mass independent) contribution of the measured gear to its transmission error, how to compute the working-surface-deviations that are the cause of any user-identified transmission-error rotational harmonic, and how to understand the relationship between such working-surface-deviations and the resultant rotational-harmonic contributions caused by these deviations.

Using computer numerically controlled (CNC) dedicated gear metrology equipment, measurements on a helical gear in sufficient detail to accurately carry out the above-described computations can take from a few to several hours. Hence, this methodology is not generally suitable for continuous production checking, but it is suitable, and is being used, for intermittent checking. Because the manufacturing errors generated by each individual manufacturing machine generally are consistent from one manufactured gear to another in a manufacturing run, it is sensible to regard the methods described herein as suitable for assessing the quality of a particular manufacturing machine, or process. Furthermore, because transmission-error contributions from working-surface errors are caused by the *collective working-surface error pattern of all teeth* on a gear, the methods described herein also may be suitable for establishing performance-based gear-accuracy standards.

The analytical relationships derived herein between tooth-working-surface-deviations and resulting transmission-error frequency spectra allow the reader to understand the causes of certain transmission-error tones, such as “sideband tones” and “ghost tones.” Moreover, because tooth damage, such as surface damage and bending-fatigue damage, cause transmission-error contributions in the same manner as manufacturing deviations, the analysis contained herein is applicable to gear-health monitoring considerations.

Because the means by which a gear must be measured to enable computation of its kinematic transmission-error contributions, and the method of kinematic transmission-error computation, both involve considerable detail, a general

orientation to the content of the book is described in the remainder of this Introduction. It is hoped this orientation might give the reader a broad perspective before he or she begins working through the details of the analysis.

1.1 Transmission Error

The transmission error of a meshing-gear-pair describes the deviation from the transmission of an *exactly constant* speed ratio. It can be displayed in the time domain as a function of the rotational position of one of the two meshing gears, or in the frequency domain. The transmission error is the principal source of vibration excitation caused by meshing-gear-pairs, for example, Mark (1992b), Smith (2003), and Houser (2007). The subject of this book is transmission-error contributions caused by geometric deviations from equispaced perfect involute surfaces of the tooth-working-surfaces of parallel-axis helical or spur gears. Because an idealized pair of parallel-axis helical gears, each with equispaced rigid perfect involute teeth would transmit an *exactly constant* speed ratio, the transmission-error contribution from each gear of a meshing-pair of nominally involute gears is the instantaneous deviation of the position of that gear from the position of its rigid perfect involute counterpart. Therefore, as described earlier in Chapter 3 by Equation (3.2), and in more detail in Chapters 5 and 7, the transmission-error contributions from each of two meshing gears are additive to yield the transmission error of the gear-pair. Consequently, especially with regard to the geometric deviations of the working-surfaces from equispaced perfect involute surfaces, it is rigorously meaningful to define and compute the transmission-error contribution arising from the geometric deviations of the working-surfaces of a single gear.

Frequency Spectrum

Vibration analyses and measurements are very often carried out in the frequency domain. It generally is impossible to directly measure the source of vibration; normally what is measured is the structural response, or in the case of noise, the acoustic response. Because the structural path between source of vibration and response measurement location is usually well modeled as a linear time-invariant system, source vibration *tones* retain their identity between source and receiver, although their amplitudes and phases are affected by the transmission media. But such media normally cause substantial changes in temporal vibration signals.

Because gears are circular and normally have equispaced teeth, dealing with their vibration signatures in the frequency domain is especially useful. Thus, dealing only with a single gear of a meshing-pair, as described above, because the gear is circular, its fundamental rotational frequency has a period of one gear rotation, and all of its harmonics are integer multiples of the fundamental frequency associated with one gear rotation.

Figure 1.1 is a sketch of the stronger harmonics that typically are observed from a single gear. The harmonic labeled 1 near the origin is the fundamental frequency associated with the rotational period of the gear. All harmonics shown are integer multiples of this fundamental rotational harmonic. If the gear has N teeth, then the

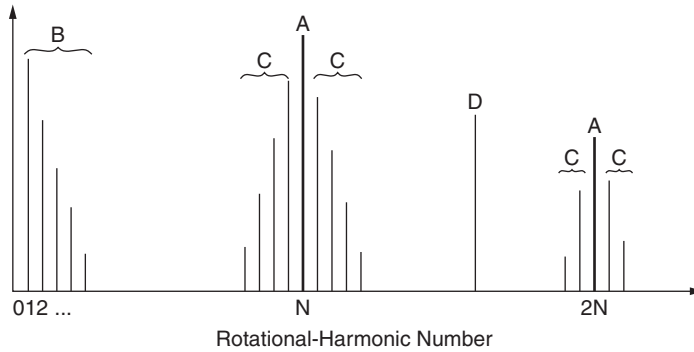


Figure 1.1 Sketch of dominant rotational harmonics caused by a single gear of a meshing-pair operating at constant speed and transmitting constant loading. Abscissa labels rotational-harmonic numbers $n = 1, 2, \dots$. The period of rotational harmonic $n = 1$ is the rotation period of the gear. All harmonics are integer multiples of $n = 1$. Rotational harmonic $n = N$ is the tooth-meshing fundamental harmonic with period equal to the gear rotation period divided by the number of teeth, N . Low-order rotational harmonics B and “sideband” harmonics C typically are strong. “Ghost tone,” when present, is labeled D (Adapted from Mark (1991))

N th rotational harmonic is the *tooth-meshing fundamental* harmonic. The period of the tooth-meshing fundamental is the gear rotation period divided by the number N of teeth. The first heavy harmonic, rotational harmonic N in Figure 1.1, is the tooth-meshing fundamental. Also shown heavy is another harmonic at rotational harmonic $2N$, which is twice the frequency of the tooth-meshing fundamental harmonic. These two harmonics are labeled A . In the neighborhoods of these tooth-meshing-harmonics are so-called “sideband rotational harmonics” labeled C . Also shown are low-order rotational harmonics $1, 2, \dots$ labeled B , and a “ghost-tone” rotational harmonic labeled D . The physical sources of all such harmonics are explained in this book. Although not shown, unless a gear is geometrically perfect, there normally will be weak contributions to all integer multiples of the rotational fundamental harmonic.

When a frequency analysis of the structural response to the vibration excitation caused by a pair of meshing gears operating at constant speed and loading is carried out, a superposition of two such spectra as that shown in Figure 1.1 is obtained. Because of the manner in which the teeth of the two gears mesh, the locations of the tooth-meshing-harmonics A from each of the two meshing gears will coincide, but generally, the locations of all other rotational harmonics will differ, because the rotation periods of the two individual gears generally will differ (unless they both have the same number of teeth).

Physical Sources of Harmonic Contributions

It is important to understand the physical sources of the various harmonics shown in Figure 1.1. If the subject gear is geometrically *perfect*, such that every tooth is

geometrically identical with no spacing errors and modified (e.g., with tip and end relief) exactly the same, then the only harmonics that would be present in Figure 1.1 would be the tooth-meshing-harmonics labeled A (assuming exactly constant rotational speed and loading). These tooth-meshing-harmonics A are caused by deviations of the elastically deformed teeth from perfect involute surfaces. Such deviations are the combined superposition of intentional (and unintentional) geometric modifications of the teeth and tooth/gearbody elastic deformations. (This fact is easily understood from the observation that if all elastically deformed tooth-working-surfaces are identical with no spacing errors, the only lack of smooth transmission is that associated with a period equal to the tooth-meshing period.) Hence, the generation of all rotational harmonics B, C, and D is caused by geometric variations of the individual tooth-working-surfaces from the mean (average) modification (intentional or otherwise) of the working-surfaces, assuming constant speed and constant loading. These deviations causing rotational harmonics B, C, and D thus are tooth-to-tooth geometric variations of the working-surfaces, including tooth-spacing errors, from the mean working-surface. Computation of the transmission-error amplitudes of these rotational harmonics, and diagnosing their working-surface sources, is the principal subject of this book. The gear measurements required to successfully accomplish this, in any specific application, also yield a very accurate three-dimensional determination of the working-surface modification, averaged over all teeth, enabling this achieved modification to be compared with that specified by the design engineer.

1.2 Mathematical Model

The mathematical analysis contained herein, leading to a systematic method for measuring a helical (or spur) gear, and computing from those measurements the locations and amplitudes of any transmission-error rotational harmonics, such as B, C, and D of Figure 1.1, has been possible because of the elegant relative simplicity of the meshing action of involute helical gears, described in more detail in Chapter 2. How this analysis has been possible can be partially understood with the aid of Figure 1.2, reproduced again as Figure 2.6.

Contact between the teeth of perfect involute helical gears takes place in a plane surface, the plane of contact shown in Figure 1.2, also called the plane of action. Real teeth have intentional modifications and manufacturing errors, however small, and they elastically deform. The (lineal) transmission error contribution from either gear in Figure 1.2 is, simply, the error in the instantaneous position of that gear, "measured" in the direction of the plane of contact of the lower figure, relative to the instantaneous position of its rigid perfect involute counterpart. The (lineal) transmission error of the gear-pair then is the superposition (algebraic sum) of the contributions from each of the two gears. Recall that rigid perfect involute gears transmit an *exactly* constant speed ratio.

It can be seen from the lower part of Figure 1.2 that, in any plane cut normal to the gear axes, tooth-pair contact takes place at a single point on each tooth. That point is in the plane of contact. When projected axially on tooth-working-surfaces,

of involute helical gear geometry has made this possible. "Linear-system analysis" methods have been utilized. The details are carried out in Chapter 7. But the book has been organized to show how gears must be measured, and transmission-error computations carried out and understood, without perhaps full comprehension of every detail of Chapter 7.

Role of Discrete Fourier Transform (DFT)

In carrying out the original analysis (Mark, 1978) that is the foundation analysis for this book, the expression for the transmission-error Fourier series coefficients, Equations (112) and (111) of that reference, could be made useful (and understandable) only by mathematically representing the tooth-working-surface-deviations as a linear superposition of "elementary errors," that is, by Equation (131) of the above-cited reference. This representation led to Equations (134) and (135) of the above-cited reference for the Fourier series coefficients of the transmission error contributions, Equation (134), expressed as a function of the discrete Fourier transform (DFT), Equation (135), of the expansion coefficients of the above-described superposition of elementary errors. (The counterparts to these equations in Chapter 7 are, respectively, Equations (7.49), (7.48), (7.50), (7.60), and (7.59).)

This original analysis, and its counterpart in Chapter 7, illustrates that the DFT (Cooley, Lewis, and Welch, 1969, 1972) is the *exact* mathematical tool required to compute, understand, and diagnose transmission-error rotational harmonic contributions, such as those illustrated by the B, C, and D contributions in Figure 1.1. As one might guess, use of the DFT arises because the working-surface geometric deviations at any fixed location on each of the tooth-working-surfaces of a gear with N teeth constitute a discrete equispaced sequence of N deviations, which because a gear is circular, is periodic with period N . The DFT is the exact mathematical tooth *required* to describe the frequency content of such phenomena. Cooley, Lewis, and Welch (1969, 1972) refer to the DFT as the "Finite Fourier Transform." Our use of its definition and properties in Chapter 4, and beyond, is consistent with that of Cooley, Lewis, and Welch.

1.3 Measurable Mathematical Representation of Working-Surface-Deviations

The above-described requirement to mathematically represent the tooth-working-surface-deviations as a linear superposition of "elementary errors" has suggested this representation method as a sensible starting point in the overall developments to be carried out. Requirements for a satisfactory representation method of tooth-working-surface-deviations are: it be capable of representing *any* deviations, that is, mathematically "complete," appropriately normalized so that expansion coefficients can be interpreted, measureable by dedicated CNC gear metrology equipment, "efficient" in some sense, and amendable to Fourier integral transformation of simple form. This last requirement is a consequence of Equation (125) of Mark (1978), which is Equation (7.62) of Chapter 7.

Among known methods of representation, two-dimensional normalized Legendre polynomials meet all of the above-mentioned requirements. If enough terms are used they can accurately represent any deviation surface, that is, they are complete, for example, Jackson (1941, pp. 63–68) and Bell (1968, p. 57). When appropriately normalized, Equations (3.13) and (3.14), their expansion coefficients can be directly interpreted, as in Equation (3.23). As a consequence of their important (unweighted) least-squares property (Jackson, 1941, pp. 215, 216) they are generally efficient. Moreover, the lowest-order two-dimensional Legendre term is a constant, representing exactly a tooth-spacing error, and the next-order linear terms represent straight-line errors commonly observed in lead (alignment) measurements and profile measurements. The Fourier integral transform of a generic Legendre polynomial is a spherical Bessel function of the first kind (Bateman, 1954, p. 122; Antosiewicz, 1964, p. 437). This very important property allows the final form of the analytical results to be represented as simply as is possible considering the complexity of the physical problem being analyzed.

Measurement Compatibility

Present-day dedicated CNC gear metrology equipment can carry out line-scanning (lead) measurements in an axial direction and line-scanning (profile) measurements in a radial direction on tooth-working-surfaces. Consequently, to obtain a representation of the working-surface-deviations over the entire rectangular working-surfaces, some sort of interpolation procedure is required to provide an (approximate) determination of the working-surface-deviations between the line-scanning measurements.

CNC gear measurement machines can be programmed to carry out such scanning measurements at any location, that is, locations of the lead-scanning measurements at any radial locations, and locations of the profile-scanning measurements at any axial locations. Consider, for example, obtaining an approximation to the working-surface-deviations utilizing only working-surface measurements provided by scanning lead measurements. Suppose scanning lead measurements are made at n different radial locations on a tooth. Then, by using the Lagrange interpolation formula (Lanczos, 1961, pp. 5, 6; Lanczos, 1956, pp. 397, 398) it is known that at any axial location, a polynomial of degree $n - 1$ can be constructed to interpolate radially across the n scanning lead measurements to provide an approximation to the profile deviations at that axial location, which will agree exactly with the n scanning lead measurements at that axial location. Then, by providing such an interpolation at each axial location, an approximation to the working-surface could be obtained everywhere, which would agree at all points on the n scanning lead measurements. But, it is possible to do much better.

To generate the Legendre expansion coefficients of the working-surface-deviations, integrations over the working-surfaces, Equation (3.20), are required. Continuing to consider lead-scanning measurements, these integrations over the working-surfaces are to be treated as iterated integrals, first along the line-scanning measurements, as in Equation (3.30), then across the line-scanning measurements, as in Equation (3.31). The accuracy of the integrals, Equation (3.30), *along* the line-scanning measurements,

is limited only by the density of sample points along the scanning lines (and the accuracy of the measurements). The second integrals, Equation (3.31), *across* the line-scanning measurements, are integrations involving the expansion coefficients obtained *along* the line-scanning measurements. We generally can expect these expansion coefficients to vary more smoothly in the direction *across* the line-scanning measurements than the raw measurements, especially in the case of the lower-order expansion coefficients.

As suggested above, these second integrations, Equation (3.31), could be carried out by utilizing the Lagrange interpolation formula to interpolate the integrands, yielding a polynomial representation of each integrand of degree $n - 1$, assuming there have been n scanning lead measurements. But a CNC gear-measurement machine can be programmed to locate the n scanning lead measurements at any radial locations. If these radial locations are chosen to be at the n zero locations of an appropriately normalized Legendre polynomial of degree n , then the accuracy achievable in the integrations is comparable to what would normally be achieved by $2n$ scanning lead measurements, for *any* radial locations of these *additional* n scanning lead measurements (Lanczos, 1956, pp. 396–400). The resulting integration procedure is called Gaussian quadrature. The above reference by Lanczos provides a very clear proof and explanation of this remarkable result. A comparable mathematically exact statement can be found in Cheney (1982, p. 110). The radial coordinate used in our analysis is “roll distance,” Equation (3.3).

The case where profile scanning measurements are used instead of lead scanning measurements is completely analogous to that described above; in this case, say m scanning profile measurements would be located axially at the zeros of a normalized Legendre polynomial of degree m .

As mentioned in Hildebrand (1974, p. 467) and shown explicitly in Mark (1983), use of Gaussian quadrature to evaluate the Legendre expansion coefficients yields Legendre polynomial expansions that agree, exactly, with the data values at the n Legendre polynomial zeros used to evaluate the expansion coefficients. That is, the resultant Legendre polynomial expansions interpolate, exactly, the data values. However, it is shown below that the Legendre polynomial expansion interpretation is the preferred interpretation.

It is known that as $n \rightarrow \infty$, the errors in Gaussian quadrature converge to zero for any continuous function (Cheney, 1982, p. 111). This behavior is in contrast to equispaced polynomial interpolation which can exhibit non-convergent oscillatory behavior (Lanczos, 1961, pp. 12, 13; Lanczos, 1956, p. 348). Consequently, all results contained in this book assume that line scanning lead and/or profile measurements are made at the zeros of appropriately normalized Legendre polynomials.

An essential requirement of a tooth-working-surface representation and measurement method is that it be capable of accurately representing sinusoidal working-surface-deviations responsible (as shown herein) for causing “ghost tones,” which are strong rotational-harmonic transmission-error tones, as illustrated by D in Figure 1.1. The lower curve in Figure 1.3 (reproduced again as Figure 3.B.2), shows a sinusoid that has been sampled by 32 samples, indicated by the small circles. The abscissa

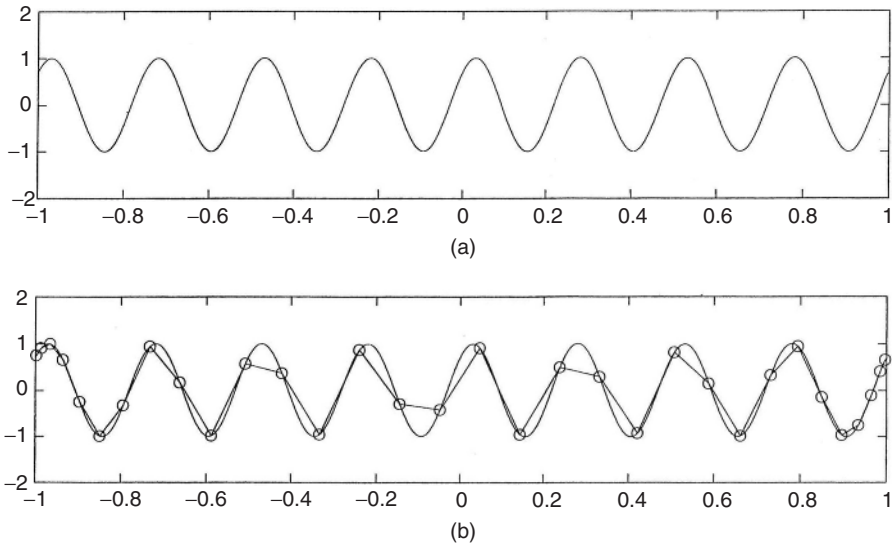


Figure 1.3 Upper curve (a) is Legendre polynomial reconstruction of the sinusoid, where the Legendre polynomial expansion coefficients were evaluated by Gaussian quadrature using only the 32 sample values of the sinusoid from the lower curve (b). Lower curve (b) shows 32 discrete samples of a sinusoid with 8 full cycles. Abscissa sample locations are the zero locations of a Legendre polynomial of degree 32 (From Mark and Reagor (2001), reproduced by permission of the American Gear Manufacturers Association)

locations of these samples are the zero locations of a Legendre polynomial of degree 32. The upper curve in Figure 1.3 is a Legendre polynomial reconstruction, where the Legendre polynomial expansion coefficients were evaluated by Gaussian quadrature using *only* the 32 sample values of the sinusoid of the lower curve. The upper curve is a virtually identical reconstruction of the lower curve, which illustrates the accuracy obtainable by utilizing Gaussian quadrature to evaluate the expansion coefficients of the Legendre polynomial reconstruction of the upper curve.

The reconstruction of the upper curve in Figure 1.3 also illustrates why the least-squares property of Legendre polynomial representations is the interpretation preferred over the above-mentioned interpolation property. Although the upper curve clearly agrees with every one of the 32 sample points of the lower curve, if given only those 32 sample points, one would be hard pressed to provide a smooth curve through them. Yet, Gaussian quadrature combined with the least-squares property of Legendre polynomial expansions provides the remarkable reconstruction shown by the upper curve. Rules are provided in Appendix 3.B for choosing the minimum number of line-scanning measurements required to accurately represent working-surface-deviations causing any ghost tone of user-specified rotational-harmonic number.

1.4 Final Form of Kinematic-Transmission-Error Predictions

The fact that meshing-gear-pairs generate tones suggests immediately the use of frequency analysis methods. Moreover, because a gear is circular, implying a fundamental rotational frequency with period equal to the gear rotational period, the frequency analysis method to be used is Fourier series. However, because the tooth-working-surface-deviations on all N teeth on a gear at any fixed location y, z on the tooth-working-surfaces, Figure 1.4, constitute an equispaced sequence of N discrete values, which are periodic with period N , the fundamental mathematical tool required to describe these deviations in the frequency domain is the discrete Fourier transform (DFT).

In Chapter 4, this DFT representation is shown by Equation (4.22) to be

$$\hat{\eta}_C(n; y, z) = \sum_{k=0}^{\infty} \sum_{\ell=0}^{\infty} B_{k\ell}(n) \psi_{yk}(y) \psi_{z\ell}(z), \quad n = 0, \pm 1, \pm 2, \dots \quad (1.1)$$

where $B_{k\ell}(n)$ is the DFT, Equation (4.21), of the expansion coefficients of the two-dimensional normalized Legendre polynomials $\psi_{yk}(y) \psi_{z\ell}(z)$ used to represent the working-surface-deviations. The above equation expresses the collective deviations (e.g., errors) of all N teeth, at each working-surface location y, z , in the frequency domain, where n is rotational-harmonic number. (The terms “deviation” and “error” are used here and everywhere in the book to describe deviations of tooth-working-surfaces from equispaced perfect involute surfaces. These deviations can include intentional modifications.) The mean-square error spectrum then is shown by Equation (4.30) to be

$$G_\eta(n) = 2 \sum_{k=0}^{\infty} \sum_{\ell=0}^{\infty} |B_{k\ell}(n)|^2, \quad n = 1, 2, 3, \dots \quad (1.2)$$

which describes, in the frequency domain as a function of rotational-harmonic number n , the collective mean-square contributions of the tooth-working-surface-deviations at all locations y, z , but not including any of the attenuating effects that would be attributable to the meshing action with a mating gear. That is, $G_\eta(n)$

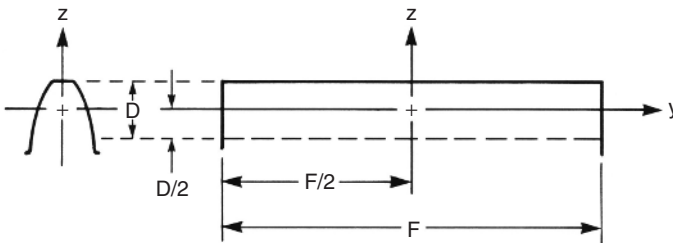


Figure 1.4 Tooth-working-surface coordinate system. The location of a generic point on the tooth-working-surfaces is described by Cartesian coordinates y, z

describes in the frequency domain only properties arising from working-surface-deviations from equispaced perfect involute surfaces.

The (complex) Fourier series coefficients of the kinematic transmission-error contributions arising from the working-surface-deviations of a single gear are given by Equation (5.16) as

$$\alpha_n = \sum_{k=0}^{\infty} \sum_{\ell=0}^{\infty} B_{k\ell}(n) \hat{\phi}_{k\ell} \left(\frac{n}{N} \right), \quad n = 0, \pm 1, \pm 2, \dots \quad (1.3)$$

Comparison of Equations (1.1) and (1.3) permits a simple interpretation of the “mesh-attenuation functions” $\hat{\phi}_{k\ell}(n/N)$. Each pair of normalized Legendre polynomial terms $\psi_{yk}(y)\psi_{z\ell}(z)$ in Equation (1.1) represents a unique two-dimensional “error pattern” on the tooth-working-surface illustrated in Figure 1.4. The amplitude of this error pattern is described in the frequency domain by $B_{k\ell}(n)$, which of course will differ for every different measured gear. By a direct comparison of Equations (1.1) and (1.3) one can conclude (correctly) that the function $\hat{\phi}_{k\ell}(n/N)$, for each Legendre $k\ell$ pair, describes the computed attenuation, in the frequency domain, of the specific error pattern characterized by the pair of normalized Legendre terms $\psi_{yk}(y)\psi_{z\ell}(z)$. This is the attenuation of working-surface-deviations that a mating gear would provide, if the measured gear were meshed with a mating gear and the transmission-error contributions arising from the measured gear were somehow measured, for example, in a single-flank test. The mean-square spectrum of the computed kinematic transmission-error contributions is given by Equation (5.18),

$$G_{\zeta}(n) = 2 |\alpha_n|^2, \quad n = 1, 2, 3, \dots \quad (1.4)$$

where α_n is given by Equation (1.3).

Especially in the case of the higher-order rotational harmonics n , the mesh-attenuation functions $\hat{\phi}_{k\ell}(n/N)$ in Equation (1.3) usually provide significant attenuation to the harmonics of the spectra $B_{k\ell}(n)$ which are caused by the unattenuated working-surface-deviations. This reduction in amplitude can be observed for each rotational harmonic n by direct comparison of the after-attenuation spectrum, Equation (1.4), with the before-attenuation spectrum, Equation (1.2). (In example computations, we compare the *rms* values of these two spectra.) However, in the case of “ghost tones,” very little, if any, attenuation is observed. It is for this reason that “ghost tones” create unwanted noise problems.

The kinematic transmission-error contributions from the measured gear are computed in the “time” domain, that is, as a function of “roll distance” x , by Equation (7.177),

$$\zeta(x) = \alpha_{0e} + 2 \sum_{n=1}^{\infty} [\alpha_{ne} \cos(2\pi nx/N\Delta) + \alpha_{no} \sin(2\pi nx/N\Delta)]. \quad (1.5)$$

The algorithms by which all computations can be carried out are summarized in Chapter 8.

Fundamental Assumptions and Parametric Dependence of Mesh-Attenuation Functions $\hat{\phi}_{k\ell}(n/N)$

To carry out the kinematic transmission-error computations it is assumed that every tooth on a gear is measured over a rectangular region, as illustrated in Figure 1.4, defined by axial facewidth F , and radial distance D determined from tip and root roll angle values by Equation (3.7). Consequently, a fundamental assumption is that the tooth-pair contact region on the subject gear is over the same rectangular region $(-F/2) < y < (F/2)$, $(-D/2) < z < (D/2)$ of every tooth on the gear. This rectangular region generally will be smaller than the full region illustrated in Figure 1.4, and is chosen by the engineer responsible for the gear measurements. Therefore, it is assumed that tooth contact with a mating gear would take place over this full rectangular region used in the gear measurements. The locations of the normalized Legendre polynomial zeros used to specify scanning lead and/or scanning profile measurement locations are then normalized to D in the case of the lead measurements and F in the case of the profile measurements, as described in Appendices 3.A and 3.B.

For any parallel-axis helical (or spur) gear of nominal involute design, this rectangular region together with the gear nominal parametric descriptions determines both the axial Q_a and transverse Q_t contact ratios, as can be seen from Equations (6.5) to (6.8). These contact ratios thus effectively describe, for any helical or spur gear, the rectangular contact region on the tooth-working-surfaces. The computed mesh-attenuation functions $\hat{\phi}_{k\ell}(n/N)$ are parametrically dependent on both Q_a and Q_t . In addition, their rotational-harmonic dependence is a function only of the ratio n/N , where N is the number of teeth. The tooth-meshing fundamental rotational harmonic is $n=N$.

Finally, it is shown in Chapter 5 by Equation (5.13), and more rigorously in Chapter 7, that if the tooth-pair stiffness per unit length of line of contact is assumed to be constant, the mesh-attenuation functions $\hat{\phi}_{k\ell}(n/N)$ are independent of tooth-pair stiffness. Consequently, in this practically important case, apart from the tooth-meshing-harmonic contributions at $n/N=1, 2, 3, \dots$, the transmission-error contributions are dependent only on the geometric working-surface-deviations from equispaced perfect involute tooth surfaces, and for any rotational-harmonic values $n=1, 2, 3, \dots$, $(n/N) \neq 1, 2, 3, \dots$ only on the axial Q_a and transverse Q_t contact ratios. These loading and inertia independent transmission-error contributions are the *kinematic* contributions to the transmission error (Merritt, 1971, p. 84).

1.5 Diagnosing Transmission-Error Contributions

Tooth-Meshing-Harmonic Contributions

The tooth-meshing-harmonic contributions A in Figure 1.1 to the transmission-error spectrum of a meshing-gear-pair operating at constant speed and constant torque are the harmonics at rotational harmonics $n=N, 2N, 3N, \dots$, where n is rotational-harmonic number of one of the meshing gears and N is the number of teeth on that

gear. These harmonics are caused by the additive contributions of the tooth-pair elastic deformations and the combined geometric deviations of the mean working-surface from a perfect involute surface of each of the two gears. The gear measurement, interpolation, and analysis methods developed in this book provide very accurate determination of the three-dimensional mean-working-surface-deviation of a measured gear, limited only by the accuracy of the CNC gear measurements. But tooth elastic deformations are not dealt with herein, and therefore, tooth-meshing-harmonic contributions to the transmission error are not computed.

Kinematic-Transmission-Error Contributions

Once any rotational harmonic n , in either a measured noise spectrum or structure-borne transducer spectrum, is identified to be of interest, the method described in Section 4.5 can be used to compute the three-dimensional working-surface error-pattern on some or all of the teeth that is the *cause* of the particular identified rotational harmonic n , that is, by Equation (4.42). To accomplish this, the working-surfaces of all teeth on the subject gear must be measured as described in Chapter 3. This computation does not require the more involved computation of the kinematic transmission-error spectrum.

However, if the rotational-harmonic n of interest is identified in the computed transmission-error spectrum, Equation (1.4), then the same computation described by Equation (4.42) is to be utilized to generate the working-surface error pattern causing the identified rotational harmonic. The resultant error pattern, computed by Equation (4.42), provides the information required to diagnose the manufacturing source of this error pattern, which is the cause of the identified rotational-harmonic tone.

Analytical approximations to the mesh-attenuation functions are described in Chapter 6 for various classes of errors, that is, accumulated tooth-spacing (index) errors, higher-order polynomial errors, and undulation errors. The behavior of these mesh-attenuation-function approximations allows one to diagnose, with some confidence, the manufacturing-error sources of low-order rotational harmonics $n = 1, 2, \dots, B$ in Figure 1.1, so-called “sideband harmonics,” C, and “ghost tones,” D.

1.6 Application to Gear-Health Monitoring

Because tooth-working-surface damage affects the transmission-error spectrum in the same way that working-surface-deviations affect it, the general results and insights provided by the analysis in this book are applicable to gear-health monitoring considerations. In particular, because damage on one tooth or a few teeth will cause only a small change to the mean-working-surface-deviation, detection methods utilizing *changes* in rotational-harmonic amplitudes, $n \neq N, 2N, \dots$, should enable the earliest detections, for example, Mark *et al.* (2010). Furthermore, because the non-tooth-meshing rotational-harmonic amplitudes of the transmission error, $n \neq N, 2N, \dots$, are almost entirely independent of tooth stiffness, these harmonic amplitudes normally are virtually unaffected by modest changes in gear loading.

Legendre polynomials provide a very efficient system for representing the working-surface-deviations caused by tooth-bending-fatigue damage (Mark, Reagor, and McPherson, 2007, Figure 5); therefore, the methods described herein can be used to compute the changes in transmission error caused by tooth-bending-fatigue damage (Mark and Reagor, 2007).

Although application to gear metrology of the overall methodology described herein utilizes normalized two-dimensional Legendre polynomials to mathematically represent tooth-working-surface-deviations, the general method of computing transmission-error contributions described in Section 7.3 initially uses a completely generic method of mathematically representing working-surface-deviations, Equation (7.50), which later is specialized to the use of Legendre polynomials, beginning with Equation (7.75). This more general representation method has been motivated, in part, because of the potential use of other working-surface-deviation representations for application in gear-health monitoring. A wide range of machinery monitoring methods can be found in Randall (2011).

1.7 Verification of Kinematic Transmission Error as a Source of Vibration Excitation and Noise

After publication of Mark and Reagor (2001) illustrating computer implementation of the gear measurement and computational methods described herein, we were asked to exercise these methods on a helical gear that we were told was responsible for causing an unwanted “ghost tone.” Because we knew the manufacturing errors causing this problem were likely to be very small, we decided to carry out two independent complete measurements of the gear using line-scanning profile and lead measurements made at the zero locations of normalized Legendre polynomials, as described in Chapter 3 of this book. Computation of the kinematic-transmission-error rotational-harmonic spectrum utilizing measurements from each of the two independent sets of measurements was carried out using the algorithms outlined in Chapter 8. If the two computed spectra were found to be in good agreement, we could be confident in our predictions of the spectra.

The measured helical gear had 51 teeth. The only information provided to us was the physical gear, the nominal design parameters of the gear, and a statement that the ghost-tone harmonic was located modestly above the tooth-meshing fundamental harmonic, $n = N = 51$. Transverse and axial contact ratios were both over 2.0.

In one of the two sets of measurements, 17 scanning profile measurements and seven scanning lead measurements were made on each tooth, and in the other set seven scanning profile measurements and 17 scanning lead measurements were made on each tooth. Because relatively good agreement of the predicted kinematic transmission-error spectrum line amplitudes was obtained from the two sets of measurements, only the prediction obtained from the measurement set using seven profile measurements and 17 lead measurements was provided to the gear owner. The dominant “ghost-tone” harmonic was found to be $n = 72$. Its computed *rms* amplitude was $0.102 \mu\text{m}$ ($4.02 \mu\text{in.}$). For the other measurement set, the computed

dominant “ghost-tone” harmonic also was $n = 72$ with a computed *rms* amplitude of $0.127 \mu\text{m}$ ($5.00 \mu\text{in.}$).

After submission of the written report to the gear owner, the acoustic spectrum, obtained by spectrum analysis of a microphone output, was provided to us by the gear owner. This noise spectrum had been obtained by operating the gear we had measured with another higher quality gear. We had no way to know the transfer function (attenuation characteristic) between the operating gears and the microphone. But we could compare our computed kinematic transmission-error spectra with that obtained from the microphone output by forcing agreement of the amplitudes of rotational harmonic $n = 72$, and comparing the remaining harmonic amplitudes obtained from the acoustic measurements and our two computations. The result of this comparison is shown in Figure 1.5, where our computed amplitudes of the neighboring harmonics in the vicinity of $n = 72$ are shown encircled. Computed and measured amplitudes are linear (not logarithmic) measure.

This example clearly demonstrates that it is possible to measure a gear in detail and compute from those measurements the rotational-harmonic location of a dominant ghost tone, $n = 72$ in this case, even for a transmission-error contribution of exceedingly small amplitude. Moreover, it has demonstrated the kinematic transmission error as a source of vibration excitation and noise. (The very small working-surface errors causing rotational harmonic $n = 72$ are delineated in Chapter 6.) Furthermore, because the subject gear had 51 teeth, rotational harmonic $n = 51$ is the tooth-meshing fundamental harmonic, which exhibits a much lower amplitude in Figure 1.5 than the ghost tone located at $n = 72$, thereby illustrating the relative importance of ghost tones in this particular example of a helical gear-pair transmitting substantial loading.

Figure 1.5 also shows good (but imperfect) correlation between computed and acoustically measured sideband rotational harmonics $n = 68\text{--}76$ in the immediate neighborhood of $n = 72$. Considering that the computed *rms* amplitude of the transmission error causing $n = 72$ is about $0.1 \mu\text{m}$ ($4 \mu\text{in.}$), it is truly remarkable that it had been possible to compute with some success these much smaller amplitude “sideband” harmonics. An explanation of how such sideband harmonics of ghost tones can be generated is found in Mark (1992a, p. 175 Case III).

1.8 Gear Measurement Capabilities

The discussion and examples provided in Chapter 6 illustrate that “ghost tones” typically are caused by periodic sinusoidal-like manufacturing errors on gear-tooth working-surfaces that are almost entirely unattenuated by the meshing action with a mating gear. In other words, such a sinusoidal (undulation) error of amplitude “*a*” will result in a kinematic transmission-error contribution of about the same amplitude “*a*.” (A reasonably complete mathematical discussion explaining this can be found in Mark (1992a), which is summarized in Section 6.6.) The above-discussed example, illustrated in Figure 1.5, therefore suggests a requirement to be able to successfully measure an undulation error with *rms* amplitude of about $0.1 \mu\text{m}$. Is this requirement reasonable? Houser (2007) shows results for a helical gear with axial and transverse

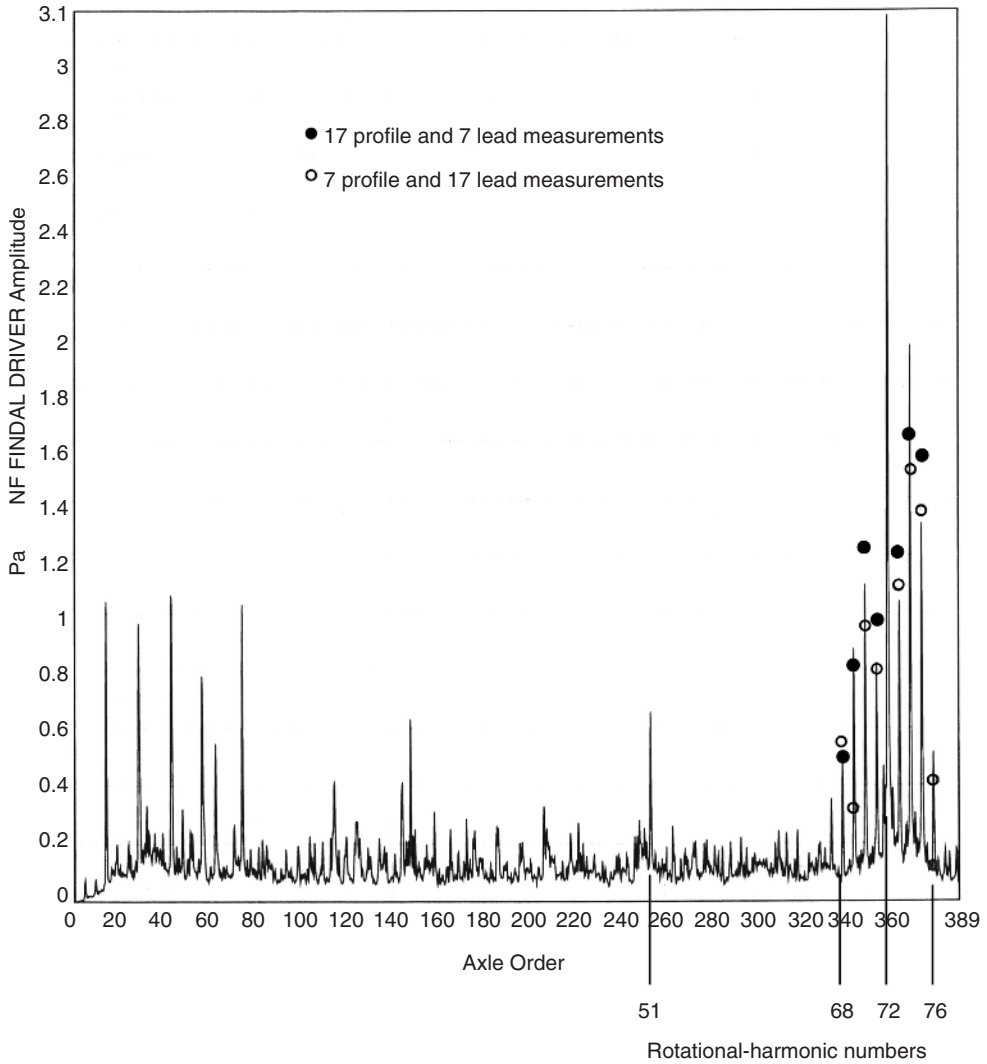


Figure 1.5 High-resolution sound spectrum generated by a 51 tooth helical gear meshing with a higher-quality gear compared with two kinematic-transmission-error spectrum computations. Both kinematic-transmission-error predictions were forced to agree with strongest acoustic-harmonic amplitude at $n=72$, thereby showing agreement of predicted rotational-harmonic amplitudes at $n=68-76$ relative to measured acoustic harmonic amplitudes. Linear-amplitude ordinate. Solid-point amplitudes computed from 17 profile and 7 lead measurements made on every tooth; hollow-point amplitudes computed from 7 profile and 17 lead measurements

contact ratios both modestly over 2.0 yielding a peak-to-peak transmission-error amplitude at design torque of slightly under $0.1\ \mu\text{m}$ ($4\ \mu\text{in.}$). This result implies one-sided transmission-error amplitude of about $0.05\ \mu\text{m}$ ($2\ \mu\text{in.}$), and an even smaller *rms* value of $0.035\ \mu\text{m}$ ($1.4\ \mu\text{in.}$). Hence, a “ghost-tone” transmission-error contribution with *rms* value of $0.1\ \mu\text{m}$ ($4\ \mu\text{in.}$) would exceed the above-mentioned amplitude, indicating that a requirement to be able to satisfactorily measure an undulation-error amplitude of about $0.1\ \mu\text{m}$ ($4\ \mu\text{in.}$), or even smaller, to be entirely reasonable. In repeated cases involving sinusoidal-like undulation errors causing “ghost tones,” we have successfully measured the gears, computed the “ghost-tone” transmission-error contributions, and the sinusoidal errors on the working-surfaces causing these ghost tones, with typical *rms* sinusoidal errors and transmission-error amplitudes of about $0.1\ \mu\text{m}$ ($4\ \mu\text{in.}$). Independent gear measurements made on the same gears, using different CNC gear-measurement machines, have yielded almost exactly the same amplitudes. Yet, the generally accepted absolute accuracy of gear metrology equipment is considered to be about $1\ \mu\text{m}$ ($39.37\ \mu\text{in.}$). A partial explanation of how the above-described “ghost-tone” measurements and computations are possible is provided below.

It was described above that the transmission-error contributions of the tooth-meshing-harmonics, labeled A in Figure 1.1, are caused by the *mean* deviation of the elastically deformed working-surfaces from equispaced perfect involute surfaces, which includes the *mean* geometric working-surface-deviations and tooth elastic deformations. The remaining rotational-harmonic contributions labeled B, C, and D are caused by geometric deviations of the individual tooth-working-surfaces from the mean-working-surface – that is, geometric tooth-to-tooth variations in the working-surfaces, including tooth-spacing errors.

Contributions of Linear-Axis Errors

The typical dedicated CNC gear-measurement machine has three linear axes, and a rotary axis on which the gear to be measured is mounted. At any *fixed* location y, z (Figure 1.4), each of the linear axes is in the same position when every tooth is measured. Therefore, a consistent position error in any linear axis will be the same for *every* measured tooth on a gear at each tooth location y, z in Figure 1.4. Consequently, *consistent* linear-axis errors provide errors in the measurement of the geometric deviation of the mean (average) working-surface-deviations, which therefore will contribute only to errors in the computed tooth-meshing-harmonic contributions of the transmission error, but will not contribute errors to the remaining computed rotational-harmonic contributions, B, C, and D in Figure 1.1.

Contributions of Rotary-Axis Errors

Now consider rotary-axis errors. In making scanning profile measurements and scanning lead measurements on a *single* tooth of either a spur or helical gear, the rotary-axis position will vary from a minimum to a maximum rotational position. The rotary-axis error at the average rotary-axis position during these measurements

can be regarded as contributing an error to the measured absolute spacing error of that tooth. *Differential* rotary-axis errors from this average rotary-axis position on each tooth will contribute to the above-described errors in the working-surface measurements from the mean (average) working-surface. That is, these differential rotary-axis errors can contribute to the computed transmission-error non-tooth-meshing rotational harmonics. But the maximum rotary-axis motion in measuring any *single* tooth is only a very small fraction of 360° . Consequently, only very short-span rotary-axis differential errors can contribute errors in computation of ghost-tone rotational harmonics. The longer span rotary-axis errors will contribute primarily to errors in (accumulated) tooth-spacing error computations.

Because a rotary scale is circular, it is useful to describe its errors using Fourier series. This decomposes its errors into a superposition of sinusoidal rotational-harmonic contributions. The effects of these rotational-harmonic rotary-axis error contributions on spur-gear transmission-error computations differs from their effects on helical-gear computations.

Consider their effects on spur-gear computations first. It can be seen directly from the involute construction described in Chapter 2, illustrated in Figure 2.3, and from the definition of transmission error given by Equation (3.2), that each rotational-harmonic amplitude of rotary-axis errors will be superimposed on the same rotational harmonic of the computed transmission error of a spur gear (with rotary-axis error amplitude proportional to base-circle radius), but with unknown phase. Hence, for successful transmission-error computations of spur gears, the higher harmonic rotary-axis errors must be minimized.

Fortunately, the effects of such rotary-axis errors are smaller on helical-gear transmission-error computations. This can be seen most easily from the stepped-gear analogy to helical gears illustrated in Figure 2.4. Because the root location of each step on the base cylinder occurs at a different cylinder rotational position, the rotary-axis higher-order rotational-harmonic error components will tend to be averaged out along the lines of tooth contact illustrated in Figures 1.2 and 3.2 in transmission-error computations. This averaging effect is likely at least partially responsible for the capability, shown herein, for successful computation of very small amplitude high order “ghost-tone” rotational-harmonic transmission-error contributions (D in Figure 1.1).

Contributions of Probe Errors

As in the case of linear-axis errors, in the case of probe errors it is convenient to distinguish consistent errors (i.e., bias errors and offset errors) from differential errors (errors in probe difference readings). Because the non-tooth-meshing rotational harmonic contributions to the transmission error are caused by geometric differences of the individual tooth-working-surfaces from the mean (average) working-surface on a gear, consistent probe errors will provide errors only to the mean-working-surface measurements, and therefore, errors only to the tooth-meshing-harmonic contributions A in Figure 1.1. Differential probe errors (errors in measurements of differences in amplitude) will provide errors to computed non-tooth-meshing rotational-harmonic amplitudes B, C, and D in Figure 1.1. Fortunately, very high quality probes are available.

Effects of Statistical Averaging

An enormous number of individual measurement samples (data values) are utilized in the computation of any transmission-error rotational-harmonic amplitude, and in computation of the working-surface-deviations that are the cause of any particular rotational harmonic. Very-short-wavelength surface-roughness characteristics and random measurement errors are averaged out in carrying out the required computations.

Summary of Required Measurement Capabilities

To be able to accurately measure and compute kinematic-transmission-error rotational-harmonic amplitudes, including “ghost-tone” amplitudes, and working-surface-deviations causing individual rotational harmonics, requirements on gear-measurement machines are:

- Linear-axis consistency (repeatability).
- Rotary-axis absolute accuracy (especially short-span high-harmonic accuracy).
- Measurement-probe consistency of bias errors and accuracy in differential measurements (measurement of differences).

Role of Working-Surface-Deviation Representation Method

Two-dimensional normalized Legendre polynomials are used in Chapter 3, and beyond, for representation of tooth-working-surface-deviations. The orthogonal property of this representation method guarantees that constant and long-wavelength measurement errors will provide *no contribution* to measured short-wavelength working-surface-deviations.

How Small is 0.1 μm (4 $\mu\text{in.}$)?

A tightly packed package of 500 sheets of copier paper is 2 in. thick. One-thousand sheets therefore is 4 in. thick, and one sheet is 4×10^{-3} in. thick. Therefore, 4×10^{-6} in. is 1/1000 of thickness of a sheet of copier paper, which is 4 $\mu\text{in.}$ (0.1 μm). Such manufacturing accuracies are at the high-end of precision grinding (Nakazawa, 1994, p. 12). The wavelength of the center of the visible spectrum of light is about 0.5 μm (20 $\mu\text{in.}$).

References

- Antosiewicz, H.A. (1964) Bessel functions of fractional order, in *Handbook of Mathematical Functions With Formulas, Graphs, and Mathematical Tables*, Chapter 10 (eds M. Abramowitz and I.A. Stegun), U.S. Government Printing Office, Washington, DC. Republished by Dover, Mineola, NY, pp. 435–478.
- Bateman, H. (1954) in *Tables of Integral Transforms*, vol. 1 (ed. A. Erdelyi), McGraw-Hill, New York.

- Bell, W.W. (1968) *Special Functions for Scientists and Engineers*, D. Van Nostrand, London. Republished by Dover, Mineola, NY.
- Cheney, E.W. (1982) *Introduction to Approximation Theory*, 2nd edn, Chelsea Publishing Company, New York.
- Cooley, J.W., Lewis, P.A.W., and Welch, P.D. (1969) The finite fourier transform. *IEEE Transactions on Audio and Electroacoustics*, **AU-17**, 77–85. Reprinted in Rabiner, L.R. and Rader, C.M. (eds) (1972) *Digital Signal Processing*, IEEE Press, New York, pp. 251–259.
- Hildebrand, F.B. (1974) *Introduction to Numerical Analysis*, 2nd edn, McGraw-Hill, New York. Republished by Dover, New York.
- Houser, D.R. (2007) Gear noise and vibration prediction and control methods, in *Handbook of Noise and Vibration Control*, Chapter 69 (ed. M.J. Crocker), John Wiley & Sons, Inc., New York.
- Jackson, D. (1941) *Fourier Series and Orthogonal Polynomials*, The Mathematical Association of America, Buffalo, New York. Republished by Dover, Mineola, NY.
- Lanczos, C. (1956) *Applied Analysis*, Prentice-Hall, Englewood Cliffs, NJ. Republished by Dover, New York.
- Lanczos, C. (1961) *Linear Differential Operators*, D. Van Nostrand Company, London.
- Mark, W.D. (1978) Analysis of the vibratory excitation of gear systems: basic theory. *Journal of the Acoustical Society of America*, **63**, 1409–1430.
- Mark, W.D. (1983) Analytical reconstruction of the running surfaces of gear teeth using standard profile and lead measurements. *ASME Journal of Mechanisms, Transmissions, and Automation in Design*, **105**, 725–735.
- Mark, W.D. (1991) Gear noise, in *Handbook of Acoustical Measurements and Noise Control*, Chapter 36 (ed. C.M. Harris), 3rd edn, McGraw-Hill, New York.
- Mark, W.D. (1992a) Contributions to the vibratory excitation of gear systems from periodic undulations on tooth running surfaces. *Journal of the Acoustical Society of America*, **91**, 166–186.
- Mark, W.D. (1992b) Elements of gear noise prediction, in *Noise and Vibration Control Engineering: Principles and Applications*, Chapter 21 (eds L.L. Beranek and I.L. Ver), John Wiley & Sons, Inc., New York, pp. 735–770.
- Mark, W.D., Lee, H., Patrick, R., and Coker, J.D. (2010) A simple frequency-domain algorithm for early detection of damaged gear teeth. *Mechanical Systems and Signal Processing*, **24**, 2807–2823.
- Mark, W.D. and Reagor, C.P. (2001) *Performance-Based Gear-Error Inspection, Specification, and Manufacturing-Source Diagnostics*, AGMA Technical Paper 01FTM6, American Gear Manufacturing Association, Alexandria, Virginia.
- Mark, W.D. and Reagor, C.P. (2007) Static-transmission-error vibratory-excitation contributions from plastically deformed gear teeth caused by tooth bending-fatigue damage. *Mechanical Systems and Signal Processing*, **21**, 885–905.
- Mark, W.D., Reagor, C.P., and McPherson, D.R. (2007) Assessing the role of plastic deformation in gear-health monitoring by precision measurement of failed gears. *Mechanical Systems and Signal Processing*, **21**, 177–192.
- Merritt, H.E. (1971) *Gear Engineering*, John Wiley & Sons, Inc., New York.
- Nakazawa, H. (1994) *Principles of Precision Engineering*, Oxford University Press, Oxford.
- Randall, R.B. (2011) *Vibration-Based Condition Monitoring*, John Wiley & Sons, Inc., Chichester, West Sussex.
- Smith, J.D. (2003) *Gear Noise and Vibration*, 2nd edn, Marcel Dekker, New York.